

www.eurjoc.org

Consecutive Three-Component Synthesis of Phenothiazine-Based Merocyanines – Bayesian Optimization, Electronic properties, and DSSC Characteristics**

Marvin Stephan, [a] Birgit Stute, [b] Eric von Lieres, [b] and Thomas J. J. Müller*[a]

Dedicated to Prof. Dr. Hans-Günther Schmalz on the occasion of his 65th birthday

A consecutive three-component Heck-Knoevenagel synthesis of phenothiazinyl merocyanines was developed by statistical design of experiments (DoE) and Bayesian optimization furnishing nine red orange dyes starting from heteroaryl halides, acrolein and ethyl cyanoacetate. Besides scrutinizing the electronic properties of these merocyanines by cyclic voltam-

metry, absorption and emission spectroscopy, and (TD)DFT calculations their saponified carboxylic acids were employed in dye-sensitized solar cell (DSSC) experiments showing promising solar cell performances with relative efficiencies of up to 93% compared to the standard ruthenium dye **N3**.

Introduction

Phenothiazine based DSSCs (dye-sensitized solar cells) have received remarkable attention in recent years.[1] The variation in their substitution pattern is restricted to the C-3, C-7 and N-10 positions of the phenothiazine core. Conjugative ligation of phenothiazine to cyanoacrylic acid, either directly or via a thiophene bridge has become the motif of phenothiazine based DSSC dyes. For the remaining positions, phenolic moieties proved to be suitable. For obtaining better solubility and introducing steric hindrance, alkyl or polyglycole chains are attached to phenolic hydroxyl groups or the phenothiazinyl nitrogen. With this molecular design sensitizers have achieved overall efficiencies of up to 9.98% and have exceeded the standard used under identical fabrication and conditions.[1b-e] The access to phenothiazine merocyanines preferentially proceeds via aldol condensation of the corresponding aldehydes with cyano acetates.[2]

Cinnamaldehyde derivatives as the starting functionality for the condensation of the donor component enable in conjunction with cyanoacetic acid the generation of extended conjugated π -systems. The expansion of the conjugated π system leads to a bathochromic shift in the longest wavelength absorption bands and also to a broader absorption in the visible range. Both effects could increase the overall performance of solar cell dyes.[3] Recently, we have disclosed a rapid and selective methodology to generate a vast library of cinnamon aldehydes by Heck reaction with various aryl bromides and $\alpha \beta$ unsaturated aldehydes and their implementation into one-pot processes.^[4] Herein, we report the optimization of the consecutive three-component Heck-Knoevenagel sequence by applying Design of Experiments (DoE). Full or fractional factorial designs are used to evaluate the impact of input variables on the yield. Based on the resulting data, a sensitivity analysis is performed, and a Gaussian Process Regression (GPR) model is trained. The GPR model is employed to predict the yield and to estimate its uncertainty across the parameter space. In the context of Bayesian optimization, further experiments are planned such as to maximize the Expected Improvement (EI).[5] The optimized protocol is applied to synthesize a series of 7donor substituted phenothiazinyl merocyanines to scrutinize their electronic properties by cyclic voltammetry, optical spectroscopy and quantum chemical calculations and to validate their suitability as photovoltaic dyes in DSSC experiments.

[a] Dr. M. Stephan, Prof. Dr. T. J. J. Müller Institut für Organische Chemie und Makromolekulare Chemie Heinrich-Heine-Universität Düsseldorf Universitätsstrasse 1, 40225 Düsseldorf, Germany E-mail: ThomasJJ.Mueller@uni-duesseldorf.de https://www.orgchem.hhu.de/

[b] B. Stute, Dr. E. von Lieres IBG-1: Biotechnology, Forschungszentrum Jülich, Wilhelm-Johnen-Str. 1, 52428 Jülich, Germany

[**] DSSC = dye-sensitized solar cell.

Supporting information for this article is available on the WWW under https://doi.org/10.1002/ejoc.202200163

© 2022 The Authors. European Journal of Organic Chemistry published by Wiley-VCH GmbH. This is an open access article under the terms of the Creative Commons Attribution Non-Commercial NoDerivs License, which permits use and distribution in any medium, provided the original work is properly cited, the use is non-commercial and no modifications or adaptations are made.

Results and Discussion

Synthesis and structure

On the way to a synthetic route for π -extended phenothiazine based merocyanines the reaction conditions for the generation of α , β -unsaturated carbonyl derivatives of phenothiazine have to be adjusted first. Thereafter, the concatenation of Heck coupling and subsequent Knoevenagel condensation in a one-pot fashion can be envisioned.

The Heck reaction with acrolein proceeds smoothly with both electron-poor and electron-rich (hetero)aromatic halides. [4] For instance, a 3-phenothiazinyl propenal can be obtained with a yield of 84%. For application as DSSC dyes long chain and branched alkyl substituents, such as 2-dodecyl tetradecyl (aka swallowtail), have already shown to be very favorable due to high hydrophobicity and the ability to suppress aggregation. [6] Under standard reaction conditions the swallowtail substituted 3-phenothiazinyl acrolein **3a** is obtained in 62% (Scheme 1). For application in a one-pot synthesis these reaction conditions require optimization. Using a sensitivity analysis based on experimental data from a fractional factorial DoE as applied in previous work, [7] the parameters amount of acrolein (2), amount of base, temperature, and time are further investigated (for all reaction conditions, see Supporting Information (SI), chapter 3.6.).

The sensitivity analysis indicates incremental effects of the selected parameters on the yield of product **3 a** (Figure 1).

The temperature shows a significant positive influence with a coefficient of 0.1 per 10 °C on the yield. The reaction time has only a small negative, but insignificant influence. Thus, the reaction time can be reduced from 4 to 3 h without a notable change of the yield. The greatest effect was seen by the added amount of acrolein (2). With a coefficient of 0.33 employing 1.9 equivalents of acrolein (2) the yield of about 85 % would be

Scheme 1. Initial reaction conditions of the Heck coupling of 3-bromophenothiazine 1 a with acrolein (2) furnishing 3-phenothiazinyl propenal 3 a.

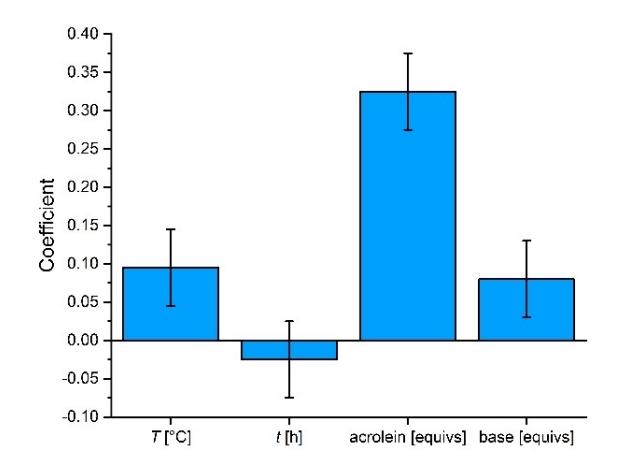


Figure 1. Sensitivity analysis of the Heck coupling of Scheme 1.

predicted. However, during the optimization experiments, only yields of 69% maximum were achieved, which is comparable to the yield under the initial conditions. The predicted sensitivity of the Heck reaction to the amount of acrolein (2) becomes particularly apparent only when the equivalents are reduced. This is caused by the symmetry of the mathematical model behind the sensitivity analysis, i.e. positive and negative parameter changes of a parameter effect the output with the same proportionality factor but with opposite signs. Nevertheless, the Heck reaction requires a significant excess of acrolein (2) and increasing the excess causes no negative effect on the yield. Since the initial base amount of 1.1 equiv. of NaHCO₃ is just above the stoichiometric minimum, a reduction to 1.0 equiv. was not deemed reasonable. Thus, only an increase was considered for this parameter, which is why the experimental plan contains only two levels (1.1 and 1.5 equiv). With a coefficient of 0.08, the base amount is shown to be significant, changing reaction conditions accordingly to a larger amount of NaHCO₃.

Based on the sensitivity analysis, the new optimal reaction conditions for Heck coupling are found: >1.5 equivalents of acrolein (2), 1.5 equivalents of NaHCO₃, reaction temperature at 110°C in a microwave reactor for a reaction time of 3 h. Although the new reaction conditions after analysis did not increase the yield, it was feasible to reduce the reaction time from 4 to 3 h by increasing the reaction temperature from 100 to 110 °C and adding an excess of base. During the sensitivity analysis, it is noticed that the palladium complex precipitates in the reaction vessel as palladium black. Therefore, the reaction conditions are adjusted to ensure a complete conversion to the corresponding acrylic aldehyde. Merely the additional addition of acrolein or catalyst, as well as the extension of the reaction time, is not sufficient (Table 1, Entry 1-5). Only when a second portion of acrolein (2) and catalyst is added after half of the reaction time (1.5 h) and reacted for another 1.5 h, a yield of 98% (¹H NMR spectroscopy) or 81% (after isolation) can be achieved (Table 1, Entry 9). In addition, upon changing the concentration the undesired double arylation is suppressed (Table 1, Entry 7–10).

With the optimal Heck conditions in hand, a suitable organocatalyst system has to be identified, prior to larger-scale optimization of the Knoevenagel condensation. Since the type of amine determines the reaction mechanism, [8] an extensive portfolio of primary, secondary, acyclic and cyclic amines and amino acids have to be investigated (Table 2).^[2,9]

L-Tryptophan as a catalyst is far superior to the other amines (Table 2, Entry 9). Significant increase of the catalyst loading shows no positive effect. Reducing the nucleophile while simultaneously increasing the reaction time leads to lower yields (Table 2, Entry 10). Thus, the starting conditions for GPR and El based optimization of Knoevenagel condensation with preceding Heck coupling are hereby set.

Bayesian optimization^[3c] is applied for improving the Knoevenagel condensation in one-pot fashion employing the synthesis of merocyanine **5 a** as a model. The utilized procedure for designing experiments for process optimization was previously described.^[7] It is based on GPR and El. The



			1a + 2 NBu ₄ Cl, DMF, 11	 	
			[Pd ₂ (dba) ₃ , <i>Cata0</i> base,		
Entry	<i>t</i> [h]	c(1 a) [M]	Acrolein 2 [equiv]	$Pd_2(dba)_3 [mol \%]$	Aldehyde 3 a [%] ^[a]
1	3	3	1.5	0.5	55
2	2×3	6	3.0	1.0	62 (80) ^[b]
3	3	6	3.0	1.0	76
4	3	6	7.5	1.0	63
5	3	6	3.0	2.0	65
6	2×1.5	6	2×3.0	1.0	53
7	2×1.5	9	2×3.0	2×1.0	82
8	2×1.5	9	2×3.0	2×1.0	80 (90) ^[b]
9	2×1.5	9	2×3.0	2×1.0	81 (98) ^[b]
10	2×1.5	9	2×1.5	2×0.5	76

Table 2. Catalyst screening for Knoevenagel condensation in a one-pot fashion. 1.0 mol% Pd₂(dba)₃ 4.0 mol% CataCXium® PtB 1.0 equiv NBu₄CI 1.5 equivs NaHCO₃ DMF, 110 °C (MW), 1.5 h then: 1.0 mol% Pd₂(dba)₃ 4.0 mol% CataCXium® PtB 3.0 equivs **2** DMF, 110 °C (MW), 1.5 h NCCH₂CO₂Et (4) 50 °C (MW). Knoevenagel condensation Catalyst [mol %] Ethyl cyanoacetate (4) [equiv] Entry Catalyst t [h] Merocyanine 5 a [%][a] NH4OAc 60 0.5 2 16 benzylamine 30 0.5 2 9 3 N,N-dimethyl-1,2-ethanediamine 30 1.5 2 9 diethylamine 2 0 4 30 0.5 piperidine 20 0.5 2 19 morpholine 0.5 2 0 6 30 7 L-lysine 30 0.5 2 5 8 L-proline 30 0.5 2 7 37 9 L-tryptophan 30 0.5 2 10 L-tryptophan 100 0.5 32 2 L-tryptophan 1.5 30 1 1 14 [a] After isolation by chromatography.

equivalents of ethyl cyanoacetate (4), reaction temperature and reaction time are taken as the main parameters for Knoevenagel condensation (Scheme 2).

For creating initial data for the GPR, the reaction conditions are chosen according to a full factorial DoE with additional reference points at the center of the observed region (Table 3, first batch of experiments, for all details, see Supporting Information, chapter 3.12.). Since the addition of ethyl cyanoacetate (4) cannot be decreased below 1.0 equiv. and a slight excess can be assumed, the lower limit of the observed region is set to 1.1 equiv. The previous catalyst screening has shown that an increase in temperature has a positive effect on the condensation. Reaction times above 0.5 h are used in the

```
1.0 mol% Pd<sub>2</sub>(dba)<sub>3</sub>
4.0 mol% CataCXium® PtB
1.0 equiv NBu<sub>4</sub>Cl, 1.5 equivs NaHCO<sub>3</sub>
DMF, 110 °C (MW), 1.5 h

then: 1.0 mol% Pd<sub>2</sub>(dba)<sub>3</sub>
4.0 mol% CataCXium® PtB
3.0 equivs acrolein (2)
DMF, 110 °C (MW), 1.5 h
then: 30 mol% L-tryptophan
NCCH<sub>2</sub>CO<sub>2</sub>Et (4), T (MW), t
```

Scheme 2. Optimization of Knoevenagel condensation in a one-pot fashion with an initial Heck reaction furnishing merocyanine **5** a.



Table 3. First batch exper	iments and values of inputs.		
Entry	Input 1 Cyanoacetate 4 [equiv]	Input 2 <i>T</i> [°C]	Input 3 <i>t</i> [h]
range of values normed range of values for DoE experiments	1.1–2 [–1, 1]	50–80 [—1, 1]	0.5–1 [–1, 1]

literature, [9] and hence the reaction space has to be investigated at longer times.

The sensitivity analysis shows a strong significant positive influence of increased amount of ethyl cyanoacetate (4), and a significant negative influence of higher temperature (Figure 2). The combination of an increased amount of nucleophile 4 and higher reaction temperature causes a strong significant dramatic loss of yield. This is not surprising since intermediate 3 a and product 5 a possess electrophilic functionalities, such as a

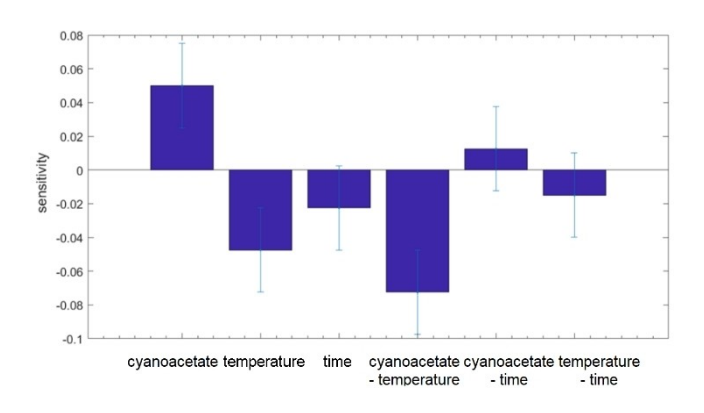


Figure 2. Sensitivity analysis of the Knoevenagel condensation step in the one-pot synthesis of merocyanine 5 a according to Scheme 2.

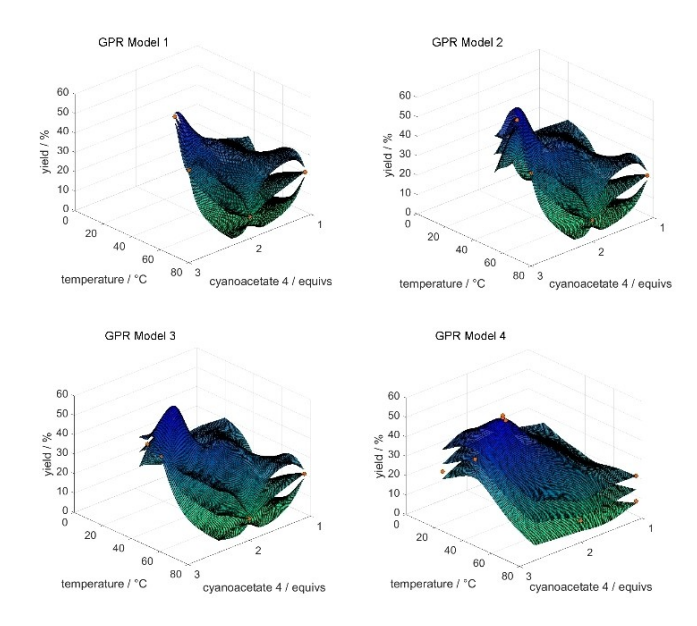


Figure 3. Graphical representation of GPR models after different steps of Bayesian optimization at $t\!=\!0.5$ h. Center plane indicates model prediction. Upper and lower planes indicate the 67% confidence interval.

carbonyl group, an ester, a cyano group and a Michael system. Increasing the reaction temperature favors competitive equilibrium reactions, which are additionally enhanced at higher ethyl cyanoacetate concentration. The reaction time has only a small and insignificant influence on the yield of merocyanine 3 a and is therefore maintained at 0.5 h.

For the second set of experiments, a full factorial DoE is chosen for the two non-fixed input parameters with limits of 2.0 to 2.3 equiv. of ethyl cyanoacetate (4) and a temperature range between 40 and 50 °C. The results are analyzed using a GPR model (Figure 3). The GPR model not only predicts the output value but also estimates the uncertainty of the model prediction. It is noteworthy to mention that a GPR estimates the uncertainty without requiring replicates of the individual measurements. The assumptions derived from the sensitivity analysis that higher concentration of cyanoacetate 4 and lower reaction temperature positively affect the yields are confirmed, but the optimum lies outside the observed range.

Hence, additional steps were planned by full factorial DoE with parameters stepwise shifted to lower temperatures and/or higher concentrations. Since the optimum falls within the observed range, in the fourth step further measurements were planned based upon the El (Figure 3). The measurement points were chosen such as to balance exploration and exploitation. Therefore, the reaction time t was again considered. The optimization is terminated after 5 steps with overall 54 experiments. At this point, the GPR model predicts no substantial improvement by further experiments. For the final model (Figure 2) two measurements are considered outliers and are excluded from the analysis.

Although additional experiments are normally expected to lead to a higher accuracy of the model, i.e. smaller error bars, the opposite is observed. This can be explained by an undefined error in the yield determination. Workup and purification for obtaining product 5a are quite error prone resulting in large variation of the yield after isolation. In the GPR context, the measurement error is not determined by replicates of the same experiment. Instead, an error is estimated for each predicted value based on the available measurement data. Both, prediction and error are updated when further data is added after each experimental step. Additional measurements are distributed between regions of high uncertainty (exploration) and regions of high performance (exploitation). In each experimental step, El provides the best compromise between exploitation and exploration (Figure 4). As a consequence, the estimated error can increase when additional data becomes available.

A z-test^[10] is applied to the final GPR model. It is a hypothesis test in which the statistic follows a normal distribution. With a probability of 80%, it can be excluded that the optimum is in the blue area (Figure 5). A large red area suggests a relatively flat optimum. The dependence of the yield on the parameters in this area turns out to be low. However, the GPR model shows the optimum for Knoevenagel condensation at 2.3 equivalents of ethyl cyanoacetate (4), $T=38\,^{\circ}\text{C}$ and $t=30\,\text{min}$ (for all details, see Supporting Information, chapter

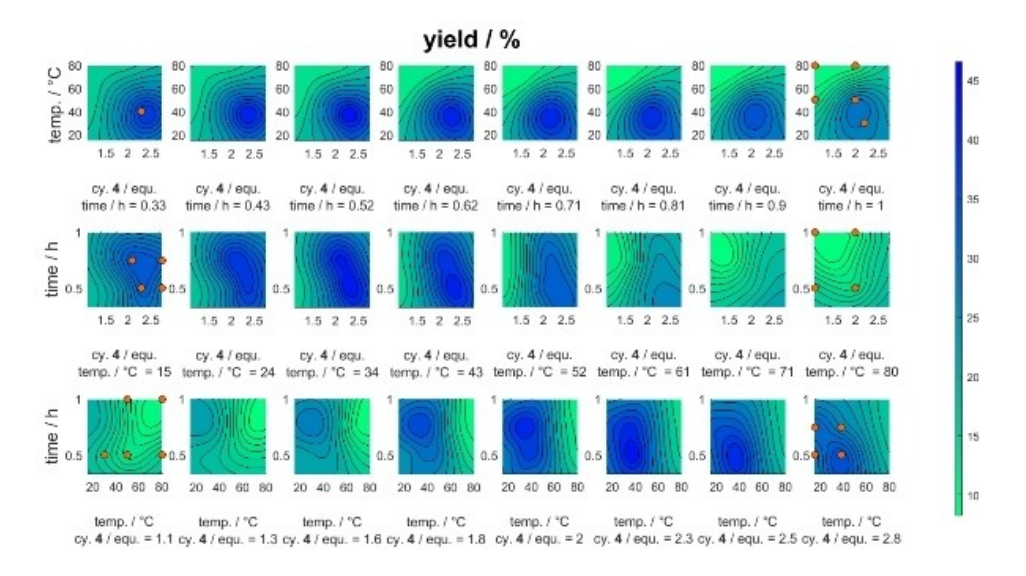


Figure 4. Graphical representation of GPR and EI based process optimization.

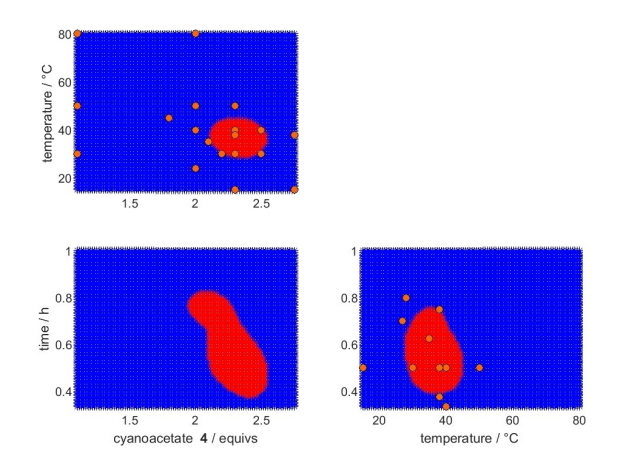


Figure 5. Significance test (z-test with confidence of 0.8) of the optimum (output: yield **5a**) for the Heck-Knoevenagel sequence (blue: negative; red: positive).

3.12.). An application of these reaction conditions finally results in a yield of 54% of merocyanine **9 a**.

The decomposition of the catalyst system for bromo phenothiazines as substrates require a second charge of catalyst and acrolein (2) for full conversion. Therefore, the more reactive iodo derivative^[11] as a substrate in the Heck step is considered. As we have shown in previous work, bromo phenothiazines can be converted to their iodo derivatives by a bromine-lithium exchange followed by quenching with iodine.^[12]

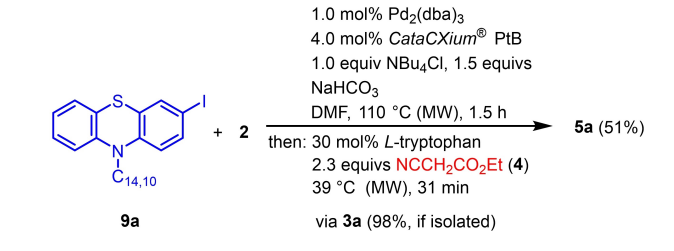
Starting from iodo phenothiazine **9a**, the reaction conditions of the Heck coupling are adjusted in a short optimization (for synthetic details, see Supporting Information, chapter 3.9.). The parameters temperature, time, and amount of acrolein **2** should be investigated. At shorter reaction time maintaining the same reaction temperature the formation of acrylic aldehyde **3a** is indeed faster than the decomposition of the catalyst. As a consequence, no second addition of catalyst and

acrolein (2) is necessary finally resulting in a yield of 98% of compound 3 a. Embedding of Heck reaction of iodo phenothazine 9 a in the Heck-Knoevenagel sequence finally gives a yield of 51% of merocyanine 5 a (Scheme 3), a similar result as for starting with the bromo phenothiazine 1 a.

Starting from 3,7-dibromo phenothiazine **1 b** or 3-bromo-7-iodophenothiazine **1 c** electron-rich 7-(hetero)aryl-3-bromo-phenothiazines **1 d**-**j** are formed in moderate to good yield by Negishi, Suzuki coupling or by the BLEBS (bromine-lithium-exchange-borylation Suzuki) sequence (Scheme 4, for synthetic details, see Supporting Information, chapters 3.2.–3.5.).^[13]

The bromo substrates 1 can be transformed into the corresponding iodo derivatives 9 by a low-temperature sequence of bromine-lithium exchange and quenching with iodine (Scheme 5, for synthetic details, see Supporting Information, chapter 3.1.).

With 7-donor 3-halophenothiazines 1 and 9 in hand the stage is set for the consecutive three-component Heck-Knoevenagel synthesis of 7-donor-substituted phenothiazinyl merocyanines 5 (Scheme 6). Starting from 3,7-dibromophenothiazine 1b or 3-bromo-7-iodophenothiazine 1c the title compounds 5 are obtained in consecutive one-pot sequence with moderate to good yield. Most interestingly, the Heck step in sequence does not affect the yields of the merocyanines.



Scheme 3. One-pot process for the synthesis of merocyanine **5 a** starting from iodo phenothiazine **9 a**.



Scheme 4. 7-Donor 3-bromophenothiazines 1 d-j.

Scheme 5. Synthesis of 7-donor-substituted 3-iodophenothiazines 9 by bromine-lithium exchange-iodolysis.

However, the iodo substrates **9** are transformed operationally more facile, since no further addition of catalyst and acrolein is required as for the bromo substrates **1**. The reason for the lower yields of the more electron-rich 7-donor substituted phenothiazinyl merocyanines can be definitely attributed to the workup and chromatography, which is notoriously challenging. The structures of the merocyanines **5** are unambiguously assigned by ¹H and ¹³C NMR spectroscopy and mass spectrometry and the molecular composition is determined by combustion analysis and/or high-resolution mass spectrometry.

The optimized reaction conditions and novel donor-substituted phenothiazine halides 1 and 9 allowed the merocyanine dyes 5 to be synthesized in a one-pot process. For the one-pot reaction starting from bromo phenothiazine 1, a two-step Heck reaction with an additional charge of Pd catalyst, ligand, and acrolein 2 is essential (Scheme 6).

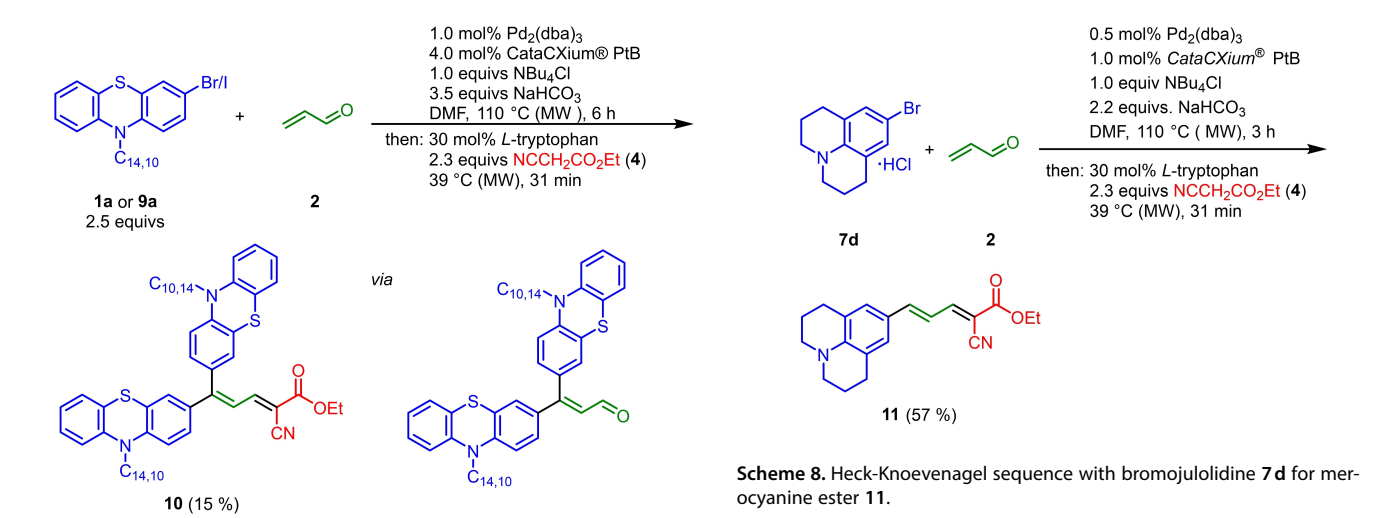
As shown in previous work, ^[4] double Heck arylation in the sense of a pseudo-three-component reaction is also feasible. Thereby, biarylated α , β -unsaturated propenals can be obtained. In the sense of a Heck-Heck-Koevenagel sequence compound 10 is obtained in 15% yield (Scheme 7). An excess of halide species resulted in a biarylated cinnamaldehyde derivative which was converted to merocyanine 5 i in the subsequent step.

Finally, also starting from julolidinylbromide hydrochloride (7 d) the Heck-Knoevenagel sequence can be successfully applied to the synthesis of julidinyl merocyanine 11 in 57% yield (Scheme 8).

The structures of the merocyanines **10** and **11** were unambiguously assigned by ¹H and ¹³C NMR spectroscopy and mass spectrometry and the molecular composition was corroborated by combustion analyses or high-resolution mass



Scheme 6. Consecutive three-component Heck-Knoevenagel synthesis of 7-donor-substituted phenothiazinyl merocyanines 5.



Scheme 7. Pseudo four-component Heck-Heck-Knoevenagel synthesis of diphenothiazine merocyanine ester **10**.

spectrometry. All merocyanines **5**, **10**, and **11** were obtained as *trans*-isomers. The double bond configuration was assigned by using occurrence of a single set of signals in ¹H NMR spectra with typical vicinal coupling constants of 11–13 Hz for the double bond protons (for further details, see Supporting Information, chapters 3.14.–3.16.).

Hydrolysis of the ethyl ester of the photosensitizers 5, 10, and 11 leads to the carboxylic acids 12, 13, and 14, which allow anchoring them to the titanium dioxide surface (Scheme 9). The molecular composition was unambiguously confirmed by high-resolution mass spectrometry.



Scheme 9. Hydrolysis of merocyanine esters 5, 10, and 11 to their carboxylic acids 12, 13, and 14.

Electronic properties

The electronic ground and excited state properties can be assessed by determining oxidation potentials by cyclic voltammetry (determined against decamethylferrocene [FeCp* $_2$]/[FeCp* $_2$] $^+$ as a standard at $E_0^{0'+1} = -95$ mV, which was itself referenced against [FeCp $_2$]/[FeCp $_2$] $^+$ at $E_0^{0'+1} = 450$ mV against Ag/AgCl^[14]), longest wavelength absorption bands by UV/Vis spectroscopy, and emission bands by fluorescence spectroscopy (Table 4).

The first oxidation potentials of the phenothiazinyl merocyanines 5 appear in a range between 482 and 850 mV and the

corresponding second oxidation potentials are found between 870 and 1560 mV (Table 4). However, the systems **5f** and **5g** are peculiar due to their diarylamino substitution, indicate that the low second oxidation potentials rather originate from the oxidation of the diarylamino substituents than from the phenothiazine core. Yet, with increasing donor strength the first oxidation potentials are cathodically shifted. The correlation of the first oxidation potentials $E_0^{0'+1}$ in the consanguineous series of merocyanines **5b-f** with Hammett parameter σ_p and the correlation of the HOMO energies E_{HOMO} first oxidation potentials $E_0^{0'+1}$ in the same series allows a prediction of electronic ground state properties based upon the phenothiazine cen-

Table 4. Selected experimental (oxidation potentials, absorption and emission bands, Stokes shifts) and calculated electronic properties of chromophores 5,	ĺ
10. and 11.	Ĺ

Compound	Oxidation po $E_0^{0/+1}$ [mV]	etentials ^[a] $E_0^{+1/+2} \text{ [mV]}$	$E_{\text{HOMO}} [\text{eV}]^{[\text{b}]}$	$K_{SEM}^{[c]}$	Absorption bands ^[f] $\lambda_{max,abs}$ [nm] (ϵ [L mol $^{-1}$ cm $^{-1}$])	Emission band ^[g] $\lambda_{max,em}$ [nm]	Stokes shift $^{ ext{[h]}}$ $\Delta ilde{v}$ [cm $^{-1}$]
5a	850	1560 ^[d]	-5.549	_[e]	248 (22000), 333 (19000), 466 (18000)	757	8200
5 b	830	1480	-5.507	$1.03 \cdot 10^{11}$	265 (24000), 335 (23000), 475 (20000)	754	7800
5 c	790	1450	-5.483	1.53·10 ¹¹	266 (27000), 337 (27000), 479 (24000)	760	7700
5 d	790	1390	-5.437	1.48·10 ¹⁰	270 (26000), 338 (24000), 480 (23000)	763	7700
5 e	669	890	-5.156	_[e]	319 (18000), 491 (10000)	658	6500
5 f ⁽ⁱ⁾	740	960	-5.225	_[e]	237 (13000), 335 (20000), 482 (8000)	734	7100
5 g ^(j)	482	680, 870 ^[k]	-4.985	_[e]	337 (51000), 488 (25000)	730	4800
10	890	1630 ^[d]	-5.230	_[e]	260 (56000), 309 (26000), 469 (25000)	761	8200
11	900	_	-5.266	_	291 (14000), 511 (39000)	584	2400

[a] Recorded in CH_2Cl_2 , T = 293 K, 0.1 M electrolyte [" Bu_4N][PF₆]; v = 100 mV/s; Pt working electrode, Ag/AgCl reference electrode, and Pt counter electrode (the potentials were determined against decamethylferrocene [FeCp*₂]/[FeCp*₂]⁺ as a standard, which was referenced against ferrocene [FeCp₂]/[FeCp*₂]⁺

 $(E_0^{0/+1}=450 \text{ mV} \text{ against Ag/AgCl})^{(14)}$ to $E_0^{0/+1}=-95 \text{ mV}$). [b] DFT calculation (PBE0/6-31G**, PCM CH₂Cl₂). [c] $K_{\text{SEM}}=10^{\frac{|(E_0^{-1}-E_1^{-1})|}{292 \text{ mV}}}$ [d] Irreversible oxidation. [e] K_{SEM} cannot be determined. [f] Recorded in CH₂Cl₂, T=293 K, $c=10^{-5} \text{ M}$. [g] Recorded in CH₂Cl₂, T=293 K, $c=10^{-6} \text{ M}$, $\lambda_{\text{exc}}=\lambda_{\text{max,abs}}$. [h] $\Delta v=\lambda_{\text{max,abs}}^{-1}-\lambda_{\text{max,em}}^{-1}$. [i] The first oxidation occurs at phenothiazine, the second on the triarylamino substituent. [j] The first oxidation $E_0^{0/+2}$ occurs on the triarylamino substituent. [k] Second and third reversible oxidations $E_0^{+2/+3}$ and $E_0^{+3/+4}$.



tered oxidations (see Supp Inf, chapters 7.1. and 7.2.). This agrees with an increase of the HOMO level of the phenothiazine core by electron releasing substituents. The semiquinone constant allows a prediction to be drawn about the stability of the cation formed. A stable cation possesses a longer lifetime in DSSC devices, allowing a better regeneration of the sensitizer upon back reduction with the electrolyte system. The K_{SEM} values^[15] of compounds $\bf 5b-d$ are typically high for phenothiazine derivatives.

The longest wavelength absorption bands of the merocyanines $\bf 5a$ and $\bf 11$ span an energy difference of $\Delta \nu = 1855~{\rm cm}^{-1}$ ($\Delta E = 0.23~{\rm eV}$), where the julolidine based merocyanine $\bf 11$ is redshifted in comparison to the phenothiazine based merocyanine $\bf 5a$ (Figure 6).

The cyanoacetate group lowers the LUMO energy and thereby shifts the HOMO-LUMO transitions to longer wave-

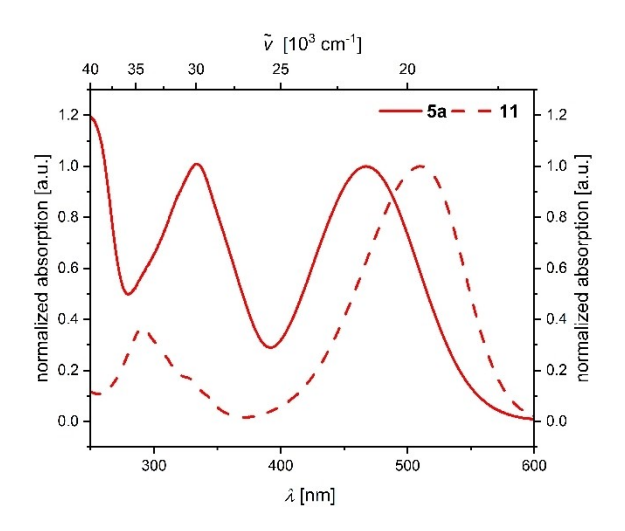


Figure 6. UV/vis absorption spectra of merocyanines **5 a** and **11** (CH $_2$ Cl $_2$, $c=10^{-5}$ M, T=298 K).

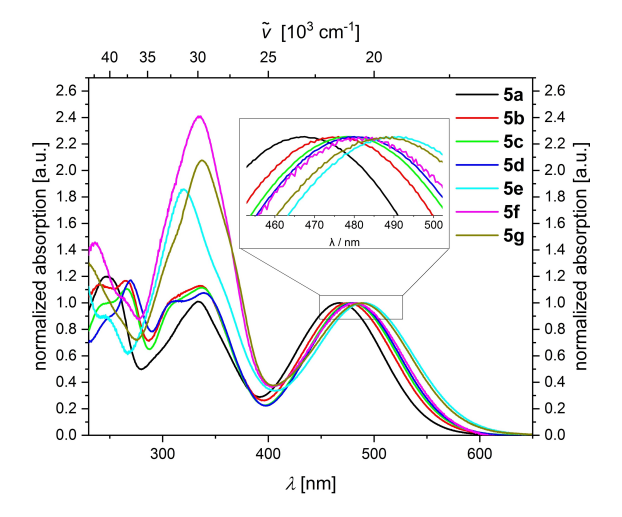


Figure 7. UV/vis absorption spectra of phenothiazine based merocyanine esters **5** and magnified long-wavelength absorption maxima (inset) (CH_2CI_2 , $c(5) = 10^{-5}$ M, T = 298 K).

lengths. The broad unstructured longest wavelength absorption bands are typical for merocyanines.^[16]

The longest wavelength absorption bands of phenothiazine chromophores **5** range from 466 to 491 nm (Table 4, Figure 7, and inset), with the most bathochromic shift caused by the *N*,*N*-dimethylaniline donor of compound **5 e**.

Linear regression correlation analysis of the longest wavelength absorption maxima in Hammett plots leads to a good fit for parameters σ_p^0 (R²=0.907) and σ_p^+ (R²=0.957) (Figure 8). The linearity of σ_p^+ underlines that the red shift of the absorption band with increasing donor strength indicates a substantial charge transfer character (Figure 8).

All phenothiazine based merocyanine dyes 5 exhibit fluorescence in the spectral range from 730 to 780 nm with phenothiazine typical Stokes shifts from 6500 to 8200 cm⁻¹ (Table 4). [2a] The energy differences between photonic excitation and the deactivation processes of the chromophores by fluorescence can be attributed to a substantial geometry change by planarization of the thiazine heterocycle and the significant dipole difference during the transition from the electronic ground state (S_0) to the excited state (S_1) . The fluorescence of most fluorophores ranges in a narrow range from 750 to 760 nm ($\Delta E = 0.02$ eV). The diarylaniline-substituted fluorophores 5f and 5g are hypsochromically shifted and appear at 730 and 734 nm, resp. Interestingly, molecule 5e containing the dimethylamino donor reveals the most hypsochromic emission of all phenothiazine merocyanines with a fluorescence band at 658 nm.

Calculated electronic structure

The electronic structure of the chromophores **5**, **10**, and **11** can be additionally scrutinized by DFT and TD-DFT calculations for assigning the experimental absorption bands. Applying *Gaussian 09*^[17] the ground state geometries were optimized using the PBE0 functional^[18] or B3LYP functional^[19,20] and Pople's 6-31G* or 6-31G** basis set.^[21] The polarizable continuum model

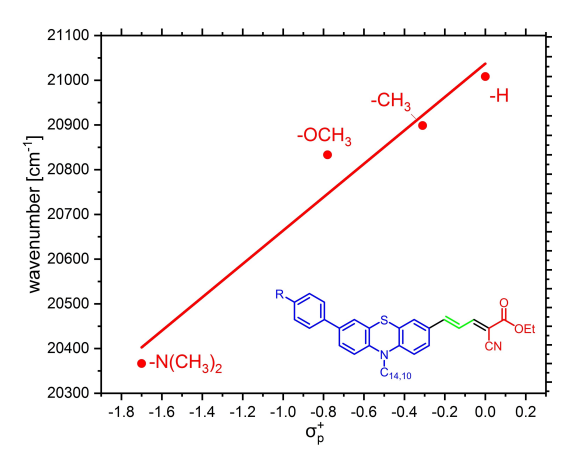


Figure 8. Plot of the wavenumbers of the long-wavelength absorption maxima of selected merocyanines **5** against Hammett parameters σ_p^+ and linear regression ($\tilde{\nu}=$ 373 cm $^{-1}\cdot\sigma_p^++$ 21037 cm $^{-1}$; $r^2=$ 0.957).



Compound	$\lambda_{max,exp}$ [nm] (ϵ [L (mol cm) $^{-1}$])	$\lambda_{max,calcd}$ [nm] (oscillator strength)	Most dominant contribution
5 a	466 (18000)	511 (0.8594)	HOMO→LUMO (99%)
	333 (19000)	369 (0.8279)	HOMO-1→LUMO (98%)
		325 (0.2037)	HOMO-2→LUMO (67 %)
	248 (22000)	277 (0.1480)	HOMO→LUMO + 3 (40 %)
5 b	475 (20000)	522 (0.9114)	HOMO→LUMO (98%)
	335 (23000)	368 (0.8827)	HOMO-1→LUMO (56%)
	265 (24000)	257 (0.4804)	HOMO-2→LUMO + 1 (66%)
5 c	479 (24000)	525 (0.9090)	HOMO→LUMO (98%)
	337 (27000)	368 (0.8739)	HOMO-3→LUMO (96%)
	266 (27000)	298 (0.4589)	$HOMO \rightarrow LUMO + 2 (43\%)$
		260 (0.5244)	HOMO-1→LUMO + 1 (43%)
5 d	480 (23000)	530 (0.8913)	HOMO→LUMO (98%)
	338 (24000)	369 (0.8965)	HOMO-2→LUMO (97%)
		305 (0.2563)	HOMO-3→LUMO (76%)
	270 (26000)	294 (0.3152)	HOMO→LUMO + 2 (42%)
		270 (0.5516)	HOMO-1→LUMO + 1 (53%)
i e	491 (10000)	567 (0.6671)	HOMO→LUMO (50%)
	,	463 (0.3096)	HOMO-1→LUMO (86%)
		370 (0.9272)	HOMO-2→LUMO (97%)
	319 (18000)	321 (0.2874)	HOMO-3→LUMO (92%)
	,	306 (0.6564)	$HOMO \rightarrow LUMO + 2 (93\%)$
5f		648 (0.2704)	HOMO→LUMO (58%)
	482 (8000)	532 (0.6279)	HOMO-1→LUMO (80%)
	(1111)	389 (1.0259)	HOMO-4→LUMO (80%)
	335 (20000)	373 (0.4766)	$HOMO {\rightarrow} LUMO + 1 \; (97\%)$
	,	336 (0.2422)	HOMO-1→LUMO + 1 (98%)
5 g		581 (0.2766)	HOMO→LUMO (96%)
3	488 (25000)	488 (0.5651)	HOMO-1→LUMO (94%)
	337 (51000)	365 (1.2133)	HOMO-4→LUMO (50%)
	(2.2.2.)	352 (0.2326)	$HOMO \rightarrow LUMO + 1 (57\%)$
		342 (0.2510)	HOMO-1→LUMO + 1 (77%)
10	469 (25000)	513 (0.2095)	HOMO-1→LUMO (66%)
-	(25000)	502 (0.4831)	HOMO→LUMO (66%)
	309 (26000)	369 (0.5226)	HOMO-2→LUMO (95%)
	223 (2000)	358 (0.1275)	HOMO-3→LUMO (93%)
11	511 (39000)	489 (1.6587)	HOMO→LUMO (100%)
•	291 (14000)	298 (0.1612)	HOMO-1→LUMO (94%)
	251 (11000)	282 (0.1529)	HOMO→LUMO + 1 (83%)

(PCM)^[22] with dichloromethane as an implicit solvent was applied since all experimental absorption and emission spectra were recorded in the same solvent. The calculated optical transitions are in good agreement with the measured spectra (Table 5). For the longest wavelength absorption bands, the HOMO-LUMO transitions dominate in most cases according to TD-DFT calculations. Chromophores **5 e**, **5 f**, and **5 g**, however, show dominant longest wavelength absorption bands that can be assigned to HOMO-1→LUMO transitions.

The deviating characteristics of the aniline based chromophores **5e**, **5f**, and **5g** with respect to their electrochemistry and photophysics can be rationalized by considering their frontier molecular orbitals (Figure 9). The direct comparison of the FMOs of the dyes **5b** and **5e** reveals that the distribution of coefficient density in the HOMO differs significantly. While the phenyl substituted dye **5b** possesses a localization on the phenothiazine core, the coefficient density in the HOMO of the dimethyaminophenyl compound **5e** resides on the benzidine moiety constituted from the aniline and the conjugated benzo fragments. In contrast, the coefficient density distribution in the LUMO is almost identical for both systems. Similarly, for diaryl

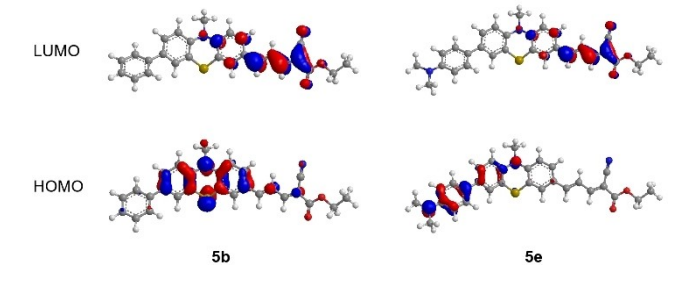


Figure 9. Frontier molecular orbitals (HOMO and LUMO) of the merocyanine esters $5\,b$ and $5\,e$ (PBE0/6-31G**, PCM CH₂Cl₂, isosurface value: 0.04 a.u.).

aniline-substituted dyes **5f** and **5g** a shift of the density distribution towards the substituent in the HOMO as for **5e** becomes apparent. Therefore, the chromophore system of aniline-substituted and strongly donor substituted merocyanines differs significantly from dyes with weaker donor substituents.



Solar cell measurements

With the dyes **12**, **13**, and **14** in hand the solar cell performances in DSSC devices can be determined (Figure 10, SI, Table S14). The photoanodes consist of nanocrystalline TiO_2 and the electrolyte is based on iodine/triiodide. The devices were prepared and the measurements were conducted according to a previously established procedure. The data of the measurements are referenced to the commercially available standard **N3** (*cis*-bis(isothiocyanato)bis(2,2'-bipyridyl-4,4'-dicarboxylato)-ruthenium(II)), which is measured under the same conditions $(\eta_{(clos)}/\eta_{(N3)})$.

The overall efficiencies η of the DSSC devices sensitized with monophenothiazine based dyes range from 3.42 (73% of N3) to 4.39 (93% of N3). The unsubstituted phenothiazine dye **12a** already achieves a good efficiency η of 4.02%. A high fill factor (FF=0.61) and good open circuit voltage (U_{OC} =686 mV) aside, the maximal power point (MPP=4016 μ W/cm²) is only 85% of the standard N3. This is due to a low short circuit current density (j_{SC} = 9.67 mA/cm²). The 4-methoxyphenyl substituent 12d gives the highest efficiency in the series almost reaching the overall efficiency of N3. In terms of voltage (MPP= 4394 μ W/cm²) and efficiency ($\eta = 4.39\%$), values in the order of a relative efficiency of 93% of the standard N3 are achieved. The open circuit voltage (U_{OC} =774 mV) exceeds the values of N3 with 58 mV. Only the short-circuit current density (j_{SC} = 11.44 mA/cm²) remains below the value of N3 with 4.41 mA/ cm². Relating the electrochemical and photophysical properties of dye sensitizers 12 to their performances in the DSSC devices, derivative 12d does not show the most bathochromic shift in the UV/vis spectrum or lowest oxidation potential, but performs above average in all areas. The absorption coefficients of all three observed absorption bands range from 23 to 26·10³ Lmol⁻¹cm⁻¹ and the first oxidation potential is 787 mV, i.e. slightly more anodically shifted than the electron-rich aryl

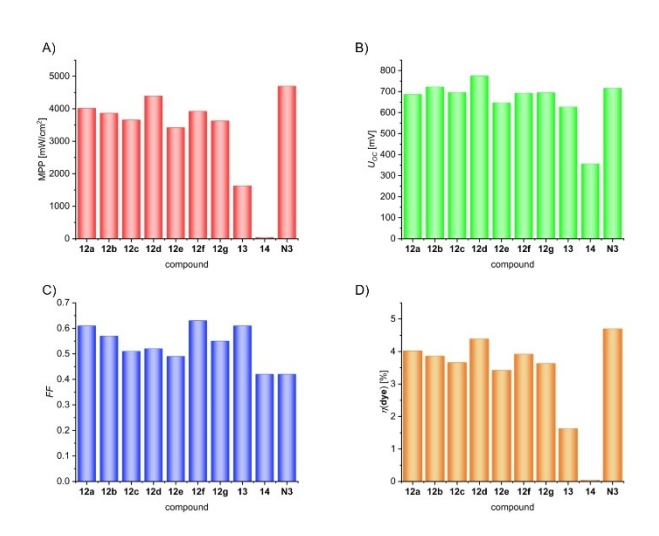
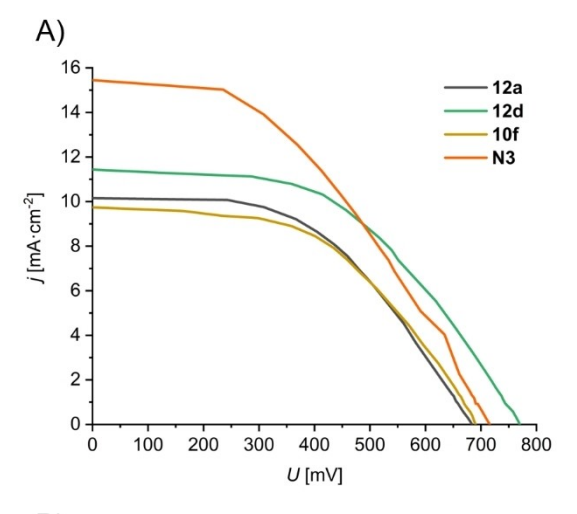


Figure 10. Comparison of selected DSSC data of dyes **12**, **13**, **14** and **N3**. A) Maximal power point (MPP). B) Open circuit voltage (U_{OC}). C) Fill factor (*FF*). D) Overall efficiencies n.

aniline derivatives. The power curve shows a more stable $(FF_{12d} = 0.52)$ than the standard $(FF_{N3} = 0.42)$.

The diarylaniline-substituted sensitizers 12 f and 12 g achieve efficiencies η of 3.92 and 3.63 %, respectively. The fill factor of chromophore 12 f (FF = 0.63) illustrates the outstanding steric shielding provided by the additional rotatable aromatics, preventing intermolecular recombination processes, but only relative efficiencies $\eta_{\rm (dye)}/\eta_{\rm (N3)}$ of 83 and 77 %, respectively, are detected compared to N3.

A DSSC device based on 12d generates the maximum short circuit photocurrent density j_{SC} of 11.44 mA/cm². The open-circuit voltages U_{OC} of the dyes 12a-g (Figure 11A, see Supporting Information, Table S14) are in the order of N3. Dye 12d ($U_{OC}=774$ mV) even exceeds the value of N3. Charge recombination in the DSSC device can reduce the open-circuit voltage, which can be compensated by sterically demanding substituents that shield the sensitizer film from the electrolyte. The open-circuit voltage of phenothiazines 12b and 12d is higher than that dyes 12f and 12g containing bulky



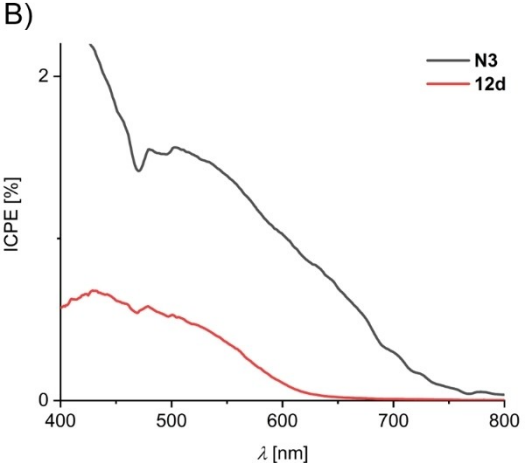


Figure 11. Comparison of selected DSSC devices **12**, and **N3**. A) Plots of the photocurrent density j vs. voltage of DSSC devices of **12a**, **12d**, **12f** and **N3** (iodine/triiodide electrolyte, AM 1.5G-irradiation with 100 mW cm⁻², at T = 293 K, thickness of the TiO_2 film of 13 μ m, irradiation area of 0.78 cm²). B) Incident photon-to-current conversion efficiency (IPCE) of selected DSSC devices **12d** and **N3** (iodine/triiodide electrolyte).



triarylamines. This phenomenon has already been observed on phenothiazine based DSSC dyes, [2a] leading to respectable efficiencies of 93% of the performance of comparable ruthenium based DSSCs despite the relatively low short-circuit current densities.

The ICPE of DSSC dye $12\,d$ shows that the photon-to-electron conversion ceases at wavelengths above 700 nm. In contrast, for N3, the photo-electron conversion does not cease up to 800 nm (Figure 11B), which, combined with lower IPCE, explains the discrepancy in photocurrents. The ICPE spectrum shows a broader spectrum than the absorption bands in the UV/vis spectrum. The broadening can be attributed to adsorption on the TiO_2 surface and the subsequent aggregate formation.

Conclusion

In summary, for the optimization of a consecutive threecomponent Heck-Knoevenagel synthesis of phenothiazinyl merocyanines a statistical DoE and Bayesian optimization based on GPR and EI was successfully employed. Sensitivity analysis of the Heck step allowed a reduction in reaction time at a higher temperature. The excess of acrolein was shown to be particularly favorable. DoE furthermore allowed a rapid identification of the relevant parameters and Bayesian optimization enabled a resource and time efficient optimization of the Heck-Knoevenagel sequence. With this optimized sequence, 9 examples of the title compounds were obtained with yields ranging from 18-54% in a one-pot fashion. These merocyanines were investigated by cyclic voltammetry and optical spectroscopy for establishing structure-property relationships. Showing correlations of the Hammett parameters of the donor substituents with the absorption band in the UV/vis spectrum were obtained. TD-DFT calculations reasonably reproduce the experimental absorption bands and allow an assignment of the absorption bands and characteristics of the electronic structure. Saponification of the phenothiazinyl merocyanines, furnish carboxylic acids that were employed as DSSC active sensitizers. The p-anisyl substituted merocyanine with an efficiency η of 4.39% ($\eta_{\text{(dve)}}/\eta_{\text{(N3)}}$ = 93%) was obtained at a short circuit current density j_{SC} of 11.44 mA/cm² and an open circuit voltage U_{OC} of 774 mV. The open-circuit voltage of this merocyanine even exceeds that of the ruthenium dye N3 by 58 mV at a lower short circuit current density, and a comparable efficiency could still be measured. Despite their relatively simple structure the title compounds promise use in DSSC devices. The ease of their diversity-oriented preparation furthermore allows optimization of the OPV behavior, which is currently underway.

Experimental Section

Details on syntheses of aryl iodides 6, aryl bromides 7, and aryl boronates 8, optimization studies, the preparation and complete characterization of phenothiazine bromides 1, cinnamaldehyde 3, merocyanine esters 5, 10, and 11, and merocyanine carboxylic acids 12, 13, and 14, Hammett correlations, DFT calculations, cyclic

voltammograms of compounds 5, 10, and 11, UV/vis spectra of compounds 5, ¹H and ¹³C NMR spectra of compounds 1, 3, 5, 6, 7, 8, 9, 10, and 11, and DSSC measurements of dyes 12, 13, and 14, are compiled in the supporting information.

Typical procedure for Heck-Knoevenagel-one-pot synthesis of merocyanine esters 5 (compound 5 d)

In a thick-walled 10 mL microwave tube, Pd₂(dba)₃ (3 mg, 1.0 mol%), CataCXium® Ptb (4 mg, 4.0 mol%), NBu₄Cl (96 mg, 0.330 mmol), phenothiazine bromide 1f (240 mg, 0.33 mmol), acrolein (2) (28 mg, 0.50 mmol), NaHCO₂ (42 mg, 0.50 mmol), and DMF (3 mL) were placed (for experimental details, see Table S10). The suspension was reacted at 110°C for 1.5 h in a microwave reactor. Subsequently, Pd₂(dba)₃ (3 mg, 1.0 mol%), CataCXium® Ptb (4 mg, 4.0 mol%), acrolein (2) (96 mg and 28 mg, 0.50 mmol) were added and reacted at 110 °C for 1.5 h. Then, L-tryptophan (20 mg, 30 mol%) and ethyl cyanocetate 4 (87 mg, 0.77 mmol) were added and the reaction solution was stirred at 39°C for 0.52 h in a microwave reactor. At the end of the reaction time, ethyl acetate (10 mL) was added and washed with saturated sodium chloride solution (3×10 mL). The aqueous solution was then also extracted with ethyl acetate (3×10 mL). The combined organic phases were dried with anhydrous magnesium sulfate and the solvent was removed under reduced pressure. The residue was adsorbed on Celite® and purified by column chromatography (eluent: n-hexane/ ethyl acetate/N.N-diethylethanamine = 100:2:2). For removing unreacted acrolein intermediates the crude product was dissolved in an ethanol-dichloromethane mixture (5:1) (10 mL), to which ptoluenesulfone hydrazide (62 mg, 0.33 mol) was added, and stirred at 20 °C for 16 h. The mixture was then removed from the solvent. The solvent was removed under reduced pressure. The residue was adsorbed on celite® and purified by column chromatography (eluent: *n*-hexane/ethyl acetate/*N*,*N*-diethylethanamine = 100:2:2) compound 5d (113 mg, 43%) was obtained as a deep red oil, R_f (hexane/EtOAc 19:1) = 0.24. ¹H NMR (600 MHz, (CD₃)₂CO): δ 0.87 (hept, $J_{HH} = 3.4 \text{ Hz}$, 6 H), 1.52–1.09 (m, 43 H), 2.03–1.95 (m, 1 H), 3.82 (s, 3 H), 3.88 (d, J_{H-H} =7.1 Hz, 2 H), 4.30 (q, J_{H-H} =7.1 Hz, 2 H), 6.98 (d, J_{H-H} = 8.8 Hz, 2 H), 7.05 (t, J_{H-H} = 8.2 Hz, 2 H), 7.17 (dd, J_{H-H} = 15.2 Hz, J_{H-H} = 11.6 Hz, 1 H), 7.36 (d, J_{H-H} = 2.1 Hz, 1 H), 7.46-7.39 (m, 2 H), 7.47 (d, J_{H-H} = 2.0 Hz, 1 H), 7.54 (d, J_{H-H} = 8.8 Hz, 3 H), 8.03 (d, J_{H-H} = 11.6 Hz, 1 H); ¹³C NMR (151 MHz, (CD₃)₂CO): δ 14.4 (2 CH₃), 14.5 (CH₂), 23.4 (CH₂), 26.8 (2 CH₂), 30.1 (4 CH₂), 30.2 (2 CH₂), 30.4 (5 CH₂), 30.5 (CH₂), 30.6 (2 CH₂), 32.0 (2 CH₂), 32.7 (CH₂), 35.4 (CH₂), 52.2 (CH₂), 55.6 (CH), 62.5 (CH₂), 103.3 (C_{quat}), 115.1 (2 CH), 115.3 (CH), 117.2 (CH), 117.9 (CH), 121.6 (CH), 125.8 (CH, C_{quat}), 126.3 (CH), 126.5 (C_{quat}), 128.1 (CH), 128.2 (2 CH), 129.6 (CH), 130.3 (C_{quat}), 132.7 (C_{quat}), 136.7 (C_{quat}), 143.8 (C_{quat}), 149.2 (CH, C_{quat}), 156.3 (CH), 160.2 (C_{quat}), 163.0 (C_{quat}); MALDI-MS (DIT, m/z): 791 ([M]⁺); IR ν [cm⁻¹]: 3034 (w), 2953 (w), 2922 (m), 2851 (m), 2725 (w), 2221 (w), 1717 (m), 1590 (w), 1562 (s), 1520 (w), 1495 (m), 1562 (s), 1520 (w), 1495 (w), 1462 (s), 1443 (m), 1408 (w), 1393 (w), 1368 (w), 1342 (m), 1242 (s), 1161 (s), 1076 (s), 1049 (m), 1040 (m), 1028 (m), 980 (m), 932 (w), 883 (w), 833 (m), 813 (m), 762 (m), 720 (w), 696 (w), 667 (w), 640 (w); Anal calcd for C₅₁H₇₀N₂O₃S (791.19): C 77.42, H 8.92, N 3.45, S 4.05; Found: C 77.40, H 9.04, N 3.40, S 3.82.

Typical procedure for syntheses of merocyanine acids 5 (compound 12 d)

Merocyanine ester $5\,d$ (111 mg, 0.14 mmol) was dissolved in a tetrahydrofuran-water mixture (6:1) (10 mL) in a *Schlenk* tube and degassed with N₂ for 30 min. Subsequently, LiOH·H₂O (138 mg, 3.30 mmol) was added and stirred for 18 h. At the end of the reaction time, acidification was performed with dilute hydrochloric



acid (pH < 3) and extracted with dichloromethane (3×10 mL). The combined organic phases were dried (anhydrous magnesium sulfate) and the solvent was removed under reduced pressure. The residue was adsorbed on Celite® and purified by column chromatography (eluent: dichloromethane/methanol = 10:1) to give compound 12 d (61 mg, 56%). HRMS calcd for $[C_{49}H_{66}N_2O_3S]^+$: 762.4794; Found: 762.4792.

Acknowledgements

The authors gratefully thank the Fonds der Chemischen Industrie and the Deutsche Forschungsgemeinschaft (Mu 1088/9-1) or financial support. We cordially thank B. Sc. Fatih Cerit (Heinrich-Heine-Universität Düsseldorf) for experimental assistance. Lars Freier is gratefully acknowledged for creating the sensitivity analysis plot of the Heck coupling. We also thank the CeMSA@H-HU (Center for Molecular and Structural Analytics @ Heinrich Heine University) for recording the mass-spectrometric and the NMR-spectroscopic data. Computational support and infrastructure were provided by the "Centre for Information and Media Technology" (ZIM) at the University of Düsseldorf (Germany). Open Access funding enabled and organized by Projekt DEAL.

Conflict of Interest

The authors declare no conflict of interest.

Data Availability Statement

The data that support the findings of this study are available from the corresponding author upon reasonable request.

Keywords: Cyclic voltammetry · DFT calculations · Heck reaction · Multicomponent reactions · Photovoltaics

- a) Y. Hua, L. T. Lin Lee, C. Zhang, J. Zhao, T. Chen, W.-Y. Wong, W.-K. Wong, X. Zhu, J. Mater. Chem. A 2015, 3, 13848–13855; b) W.-I. Hung, Y.-Y. Liao, T.-H. Lee, Y.-C. Ting, J.-S. Ni, W.-S. Kao, J. T. Lin, T.-C. Wei, Y.-S. Yen, Chem. Commun. 2015, 51, 2152–2155; c) R. Y.-Y. Lin, F.-L. Wu, C.-T. Li, P.-Y. Chen, K.-C. Ho, J. T. Lin, ChemSusChem 2015, 8, 2503–2513; d) Y. Hua, S. Chang, D. Huang, X. Zhou, X. Zhu, J. Zhao, T. Chen, W.-Y. Wong, W.-K. Wong, Chem. Mater. 2013, 25, 2146–2153; e) J.-S. Luo, Z.-Q. Wan, C.-Y. Jia, Chin. Chem. Lett. 2016, 27, 1304–1318.
- [2] a) T. Meyer, T. J. J. Müller, Org. Mater. 2020, 2, 64–70; b) T. Meyer, R. Krug, T. J. J. Müller, Molecules 2021, 26, 5149; c) H. Tian, X. Yang, R.

- Chen, Y. Pan, L. Li, A. Hagfeldt, L. Sun, *Chem. Commun.* **2007**, 3741–3743.
- [3] a) Z.-S. Wang, Y. Cui, Y. Dan-oh, C. Kasada, A. Shinpo, K. Hara, J. Phys. Chem. C 2007, 111, 7224–7230; b) K. Hara, M. Kurashige, S. Ito, A. Shinpo, S. Suga, K. Sayama, H. Arakawa, Chem. Commun. 2003, 252–253; c) T. Kitamura, M. Ikeda, K. Shigaki, T. Inoue, N. A. Anderson, X. Ai, T. Lian, S. Yanagida, Chem. Mater. 2004, 16, 1806–1812; d) Near-Infrared Dyes for High Technology Applications, (Eds.: U. Resch-Genger, S. Daehne, O. S. Wolfbeis), Vol. 52, Springer, Dordrecht, Netherlands, 1998.
- [4] M. Stephan, J. Panther, F. Wilbert, P. Ozog, T. J. J. Müller, Eur. J. Org. Chem. 2020, 2086–2092.
- [5] M. J. Anderson, P. J. Whitcomb, RSM Simplified: Optimizing Processes Using Response Surface Methods for Design of Experiments, CRC Press, New York, 2005.
- [6] a) T. Meyer, D. Ogermann, A. Pankrath, K. Kleinermanns, T. J. J. Müller, J. Org. Chem. 2012, 77, 3704–3715; b) M. Kastler, W. Pisula, D. Wasserfallen, T. Pakula, K. Müllen, J. Am. Chem. Soc. 2005, 127, 4286–4296.
- [7] a) L. Freier, J. Hemmerich, K. Schöler, W. Wiechert, M. Oldiges, E. von Lieres, Eng. Life Sci. 2016, 16, 538–549; b) H. Morschett, L. Freier, J. Rohde, W. Wiechert, E. von Lieres, M. Oldiges, Biotechnol. Biofuels 2017, 10, 26.
- [8] K. van Beurden, S. de Koning, D. Molendijk, J. van Schijndel, Green Chem. Lett. Rev. 2020, 13, 349–364.
- [9] Hu, Y.-H. He, Z. Guan, Catal. Commun. 2010, 11, 656-659.
- [10] R. A. Fisher, Statistical Methods for Research Workers, Oliver and Boyd, Edinburgh, 1932.
- [11] H. M. Senn, T. Ziegler, Organometallics 2004, 23, 2980-2988.
- [12] a) M. Sailer, R.-A. Gropeanu, T. J. J. Müller, J. Org. Chem. 2003, 68, 7509–7512; b) M. Hauck, M. Stolte, J. Schönhaber, H.-G. Kuball, T. J. J. Müller, Chem. Eur. J. 2011, 17, 9984–9998.
- [13] A. W. Franz, T. J. J. Müller, Synthesis 2008, 1121–1125.
- [14] P. Zanello, In Ferrocenes; A. Togni, T. Hayashi, eds.; Wiley VHC: Weinheim, Germany, 1995, p. 317.
- [15] J. H. Baxendale, H. R. Hardy, J. Chem. Soc. Faraday Trans. 1953, 49, 1433– 1437.
- [16] H. A. Shindy, Dyes Pigm. 2017, 145, 505-513.
- [17] M. J. Frisch, G. W. Trucks, H. B. Schlegel, G. E. Scuseria, M. A. Robb, J. R. Cheeseman, G. Scalmani, V. Barone, G. A. Petersson, H. Nakatsuji, X. Li, M. Caricato, A. Marenich, J. Bloino, B. G. Janesko, *Gaussian 09, Revision A.02*. Gaussian Inc., Wallington CT, 2016.
- [18] C. Adamo, V. Barone, J. Chem. Phys. 1999, 110, 6158-6170.
- [19] a) A. D. Becke, J. Chem. Phys. 1993, 98, 1372–1377; b) A. D. Becke, J. Chem. Phys. 1993, 98, 5648–5652.
- [20] a) C. Lee, W. Yang, R. G. Parr, *Phys. Rev. B* 1988, *37*, 785–789; b) K. Kim, K.
 Jordan, *J. Phys. Chem.* 1994, *98*, 10089–10094; c) F. J. Devlin, J. W. Finley,
 P. J. Stephens, M. J. Frisch, *J. Phys. Chem.* 1995, *99*, 16883–16902.
- [21] R. B. J. S. Krishnan, J. S. Binkley, R. Seeger, J. A. Pople, J. Chem. Phys. 1980, 72, 650–654.
- [22] G. Scalmani, M. J. Frisch, J. Chem. Phys. 2010, 132, 114110.
- [23] a) H. Zhang, J. Fan, Z. Iqbal, D.-B. Kuang, L. Wang, D. Cao, H. Meier, *Dyes Pigm.* 2013, 99, 74–81; b) B. C. O'Regan, J. R. Durrant, *Acc. Chem. Res.* 2009, 42, 1799–1808; c) D. P. Hagberg, J.-H. Yum, H. Lee, F. De Angelis, T. Marinado, K. M. Karlsson, R. Humphry-Baker, L. Sun, A. Hagfeldt, M. Grätzel, M. K. Nazeeruddin, *J. Am. Chem. Soc.* 2008, 130, 6259–6266.

Manuscript received: February 14, 2022 Revised manuscript received: March 24, 2022 Accepted manuscript online: March 31, 2022